J Sol-Gel Sci Techn (2007) 42:257–263
DOI 10.1007/s10971-006-0201-y

# UV assisted pyrolysis of solution deposited $BiFeO_3$ multiferroic thin films. Effects on microstructure and functional properties

**S. Habouti · C.-H. Solterbeck · M. Es-Souni**

Published online: 17 October 2006


**Abstract** $BiFeO_3$ thin films were processed on platinized silicon substrate via chemical solution deposition. Short wave UV assisted pyrolysis was conducted in oxygen atmosphere in order to obtain a fine and homogeneous grain structure. Phase pure thin films with a pronounced (100) texture were obtained at a fairly low annealing temperature of 600°C. For comparison specimens processed without UV assisted pyrolysis were also investigated. It is shown that UV assisted pyrolysis leads to a substantial improvement of leakage resistance properties. Polarization switching could also be obtained using capacitance-voltage (C-V) curves. The leakage current was investigated as a function of temperature. Interpretation in terms of Frenkel-Poole mechanism leads to a high trap depth in the range of 2.4 eV which is attributed to the creation of $Fe^{2+}$ centres. For both microstructures investigated well saturated magnetization loops were obtained with a remnant magnetization of $2Mr = 5.4$ emu/cm$^3$ and a coercive fields in the range of $2Hc = 200$ Oe. Slightly higher saturation magnetization 2Ms of 55.4 emu/cm$^3$ was obtained for UV assisted pyrolysis in comparison to 45.8 emu/cm$^3$ for the thin films processed without UV.

**Keywords** Multiferroic · $BiFeO_3$ · Dielectric properties · Ferroelectric properties · Leakage current · Magnetic properties

S. Habouti · C.-H. Solterbeck · M. Es-Souni (✉)
Institute for Materials and Surface Technology (IMST), Kiel University of Applied Sciences,
Grensztrasse 3, D-24149 Kiel, Germany
e-mail: me@fh-kiel.de

## 1 Introduction

$BiFeO_3$ (BFO) is a perovskite type material with a rhombohedrally distorted cell which belongs to the polar *R3c* space group. This material is known to be ferroelectric with a high Curie transition temperature $T_c$ of 810°C and antiferromagnetic with a Neel temperature of 380°C [1–3]. The coupling between magnetic and electrical order parameters and the high transition temperatures involved make this material promising for technological applications including new memory devices and lead-free piezoelectrics [4]. During the last years, increasing attention has been devoted to BFO thin films [4–12]. BFO heteroepitaxial films were processed via pulsed laser ablation (PLD) [4] and metalorganic chemical vapor deposition [5] on $SrTiO_3$-single crystal/$SrRuO_3$ as well as on platinized silicon buffered with a $LaNiO_3$ layer using RF magnetron sputtering [6]. Polycrystalline films were obtained on platinized silicon using sol-gel or PLD routes [7–14]. While well saturated polarization hysteresis loops with high remnant polarization and low leakage currents were reported for PLD films, sol-gel films have been in contrast found to have a large scatter in the polarization properties. Hysteresis loops which rather resemble those of a leaky dielectric [11, 12] and well saturated ones [8–10] were reported on platinized silicon, depending on testing temperature and stoichiometry. It seems that the processing conditions like annealing temperature and annealing atmospheres [9] as well as doping, particularly using lanthanide elements [8], play a prominent role in controlling the polarization properties. Furthermore the films are generally characterized by low break down fields and poor leakage current properties [11] at room temperature, and this might be a concern, particularly as to the relevance of the high remnant polarization properties reported for BFO films [4–6, 8–10]. Although chemical solution deposition (CSD) is a well established

processing method for ceramic thin films, offering many advantages, e.g. easy control of microstructure and stoichiometry, more work is needed to establish appropriate processing routes for high quality BFO films, including precursor solution, pyrolysis and annealing conditions as well as substrate choice.

In the present work a new processing route for BFO thin films using UV short wave light is presented. The method is inspired from a previous work by Chang et al. [15], who used it to process barium strontium titanate thin films at lower annealing temperatures and reduced the leakage current. This method has also been used by Calzada et al. [16] for UV assisted sol-gel processing of $PbTiO_3$ based ferroelectric thin films to improve the crystallinity at lower processing temperatures as required by silicon integrated circuit technology. The results obtained in this paper show that the use of UV light to aid pyrolysis results in a substantial improvement of the ferroelectric properties and reduction of leakage current.

## 2 Experimental methods

For the preparation of BFO precursor solution bismuth (III) acetate ($C_6H_9O_6Bi$, Strem Chemicals, USA) and iron (III) acetylacetonate ($C_{15}H_{21}FeO_6$, Fluka, Germany) were dissolved in deionized water and acetic acid mixed in 1:2 volume ratio. The final concentration of the precursor was 0.25 mol/l. No Bi-excess was used in contrast to earlier work [13, 17]. The precursor solution was spin-coated on a platinized silicon substrate ((111)Pt/Ti/$SiO_2$/Si, Inostek, South Korea) at 5000 rpm. For pyrolysis a UV chamber with in- and outlet valves for oxygen, and comprising a UV lamp (150 W, wavelength $\lambda$ between 350 and 400 nm) and a small hot plate was used. Each layer was pyrolysed in the UV chamber under an oxygen atmosphere at 300°C for 10 min and then annealed under oxygen atmosphere in a pre-heated tube furnace at 600°C for 6 min before the second layer was processed. After these deposition cycles the film was fired for 60 min in the furnace at 600°C. Thin BFO films of ellipsometric thicknesses of 80 and 250 nm were obtained after deposition of 2 and 6 layers, respectively (complex refraction index: $n^* = 2.82 + 0.06j$). For comparison specimens were processed without UV assisted pyrolysis, keeping otherwise the same conditions. The specimens are designated UVP and NP respectively for UV assisted pyrolysis and hot-plate pyrolysis in air.

Microstructure was analysed using X-ray diffraction (XRD). Atomic force microscopy (AFM) investigations were conducted in non-contact mode on a commercial AFM (SIS GmbH, Herzogenrath, Germany).

For electrical measurements, round platinum front electrodes of 0.6 mm diameter (area $2.8 \times 10^{-3}$ $cm^2$) were sputtered and subsequently annealed for 15 min at 400°C in order to heal out eventual defects due to sputtering. The polarization hysteresis properties were investigated at room temperature by Radiant Technology RT6000S. The dielectric properties were obtained using a computer-controlled Agilent 4192A impedance analyzer at driving signal amplitude of 25 mV.

Voltage- and temperature-dependent leakage currents were measured using a computer controlled set-up including a high-precision electrometer (Keithley 6517A) and a heating stage which allows the temperature to be controlled with an accuracy of 0.2 K. Current density-voltage ($J$–$V$) characteristics were acquired in the step mode with a delay time of 30 s to allow for sample discharging. The signal was applied to the bottom electrode in all cases and the voltage step was 0.2 V. The temperature was measured with a thermocouple placed on the sample surface. Heating was performed using a computer controlled heating stage.

The magnetic properties were characterized by means of a vibrating sample magnetometer (VSM, ADE, Pittsburgh, PE). The magnetization was obtained for each field value from an average of 100 measurements.

## 3 Experimental results and discussion

### 3.1 Microstructure

Figure 1 shows the XRD patterns of both microstructures processed. In both cases pure perovskite phase films with polycrystalline structures were obtained. However, the XRD patterns of UVP suggest better crystallinity, as can be inferred from the high peak intensities obtained. The degree of the (100) orientation, $F$, was estimated by the Lotgering's [18] method: Diffraction peaks that do not coincide with those of the Pt-substrate and in the range of $20 \leq 2\theta$

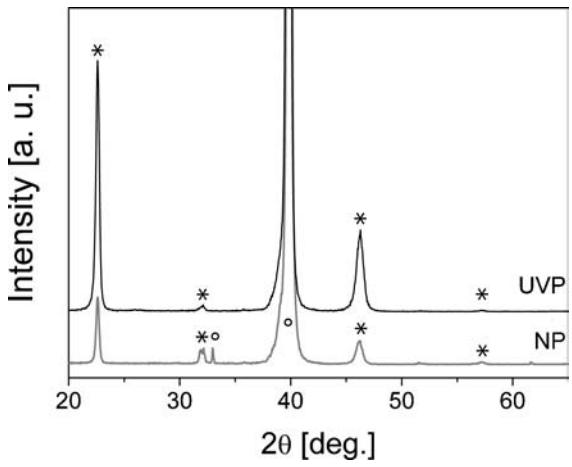


**Fig. 1** XRD patterns of the BFO thin films pyrolysed with (UVP) and without UV (NP). The stars are for BFO, and the circles for substrate

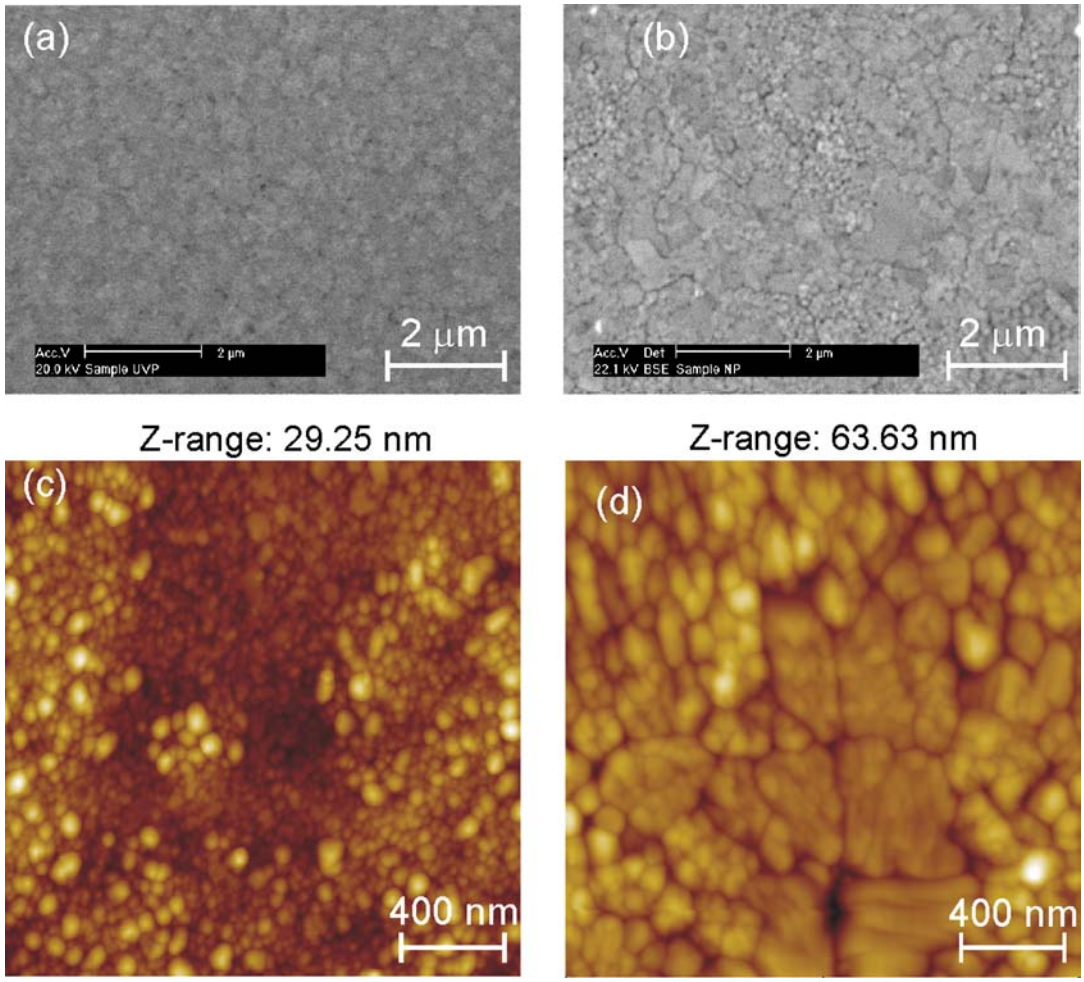


**Fig. 2** Back-scattered scanning electron micrographs (a,b) and AFM micrographs (c,d) of the surface topography of the BFO films. UVP (a,c) and NP (b,d)

$\leq 65^\circ$ were used for the calculation. The degrees of (100) orientation $F$ are 0.95 for the sample UVP and 0.55 for the sample NP. The specimen UVP shows a very strong preferred (100) orientation. This is rather surprising since (111) oriented films are normally expected if one would consider (111)- BFO plane matching with (111)-Pt ($d_{111} = 0.227$ nm for Pt and $d_{111} = 0.228$ nm for BFO) where mismatching is very small in contrast to(100)-BFO on the (111)-Pt terminated substrate ($d_{100} = 0.132$ nm for BFO). It seems that UV assisted pyrolysis favours the formation of a template layer which then entails the texture of the film. This strong effect on the orientation is very much similar to that found in $Pb(Zr_x, Ti_{1-x})O_3$ thin films processed on the same substrate heterostructure using the same conditions of UV-assisted pyrolysis as above [19]. Reports on microstructure development of PZT attribute the formation of specific textures to incipient template layers, the stoichiometry and structure of which are still the subject of controversy [19–21]. Intermetallics, PbO [20] and oxygen deficient pyrochlores [21] have all been accepted responsible for the formation either of (111) or (100) textures. Studies concerned with microstructure development of sol-gel BFO films are not yet available, and we can only speculate that the nucleation of the perovskite phase is not governed by interfacial kinetics, i.e. lowering of the interfacial energy, since none of the possible template layers (Bi-Pt, Fe-Pt intermetallics, Bi-oxides) would match (100)-BFO. Rather nucleation and growth along planes involving lower lattice distortions [4], e.g. (100), may control microstructure. But more studies dealing with different pyrolysis temperatures and conditions and their effects on microstructure control are needed in order to understand the microstructure development of sol-gel BFO films.

Preliminary observation of surface topography using the back scattered electrons imaging mode of the scanning electron microscope (SEM) revealed crack-free films with smooth topography. Figure 2(a) shows an almost featureless surface for UVP whereas Fig. 2(b) illustrates the somewhat

coarse and bimodal grain microstructure of NP. Figure 2(c–d) shows AFM micrographs of the surface morphologies of both specimens, and confirms the SEM observations. A fine grained structure with a smooth surface topography is obtained for the UVP, in contrast to the coarse and somewhat rougher grain morphology exhibited by NP. The root mean square (rms) roughness obtained is 4 and 6 nm for UVP and NP, respectively. As discussed by Calzada et al. [16] the early cracking of the C–H bonds and the resulting efficient pyrolysis due to the existence of highly activated oxygen species, are supposed to lead to incipient nuclei formation and crystallization, probably via the formation of a metastable precursor phase. It is beyond the scope of this work to discuss possible effects of UV radiation on thin film crystallization. This needs more investigations using appropriate techniques such as transmission electron microscopy and XPS analysis in order to elucidate the mechanisms of early film formation.

### 3.2 Dielectric and ferroelectric properties

The frequency dependence of the dielectric constant and dielectric loss are shown in Fig. 3. The values lie in the range of those reported in previous work [8, 13, 17, 22].The dielectric properties, i.e. the dielectric constant and the dielectric loss, are somewhat lower for UVP in comparison to NP. But this can be attributed to the lower conductivity of UVP specimens (see below), and the values obtained probably reflects more the real one in comparison to that of NP. In fact the higher conductivity of NP may lead to an apparently higher dielectric constant, as may be found in ref. [23, 24]. Also it is seen that the frequency dispersion of the dielectric constant is quite low, and suggests homogeneous thin film stoichiometry.

The dependence of the dielectric constant on DC bias field (dielectric constant-electric field ($\varepsilon'$-E) or capacitance-voltage (C-V) curves) could only be measured for UVP, and is displayed in Fig. 4. The high leakage current found for

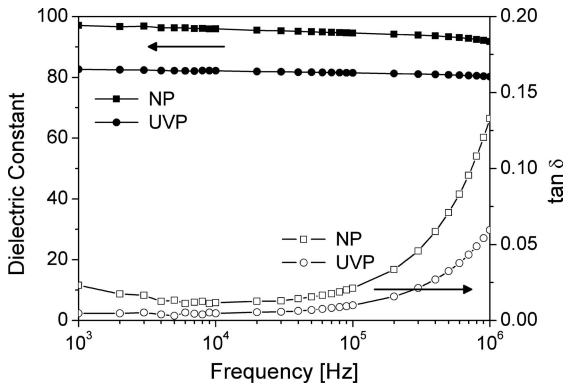


**Fig. 3** Frequency dependence of the dielectric constant and the dielectric loss of the Pt/BFO/Pt capacitors. Film thickness was 250 nm

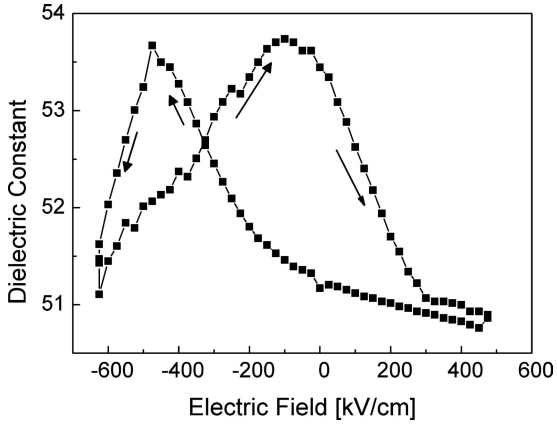


**Fig. 4** DC bias field dependence of the dielectric constant of a 80 nm UVP thin film. The curve was obtained at 30 kHz and an oscillation voltage amplitude of 25 mV. Film thickness was 80 nm

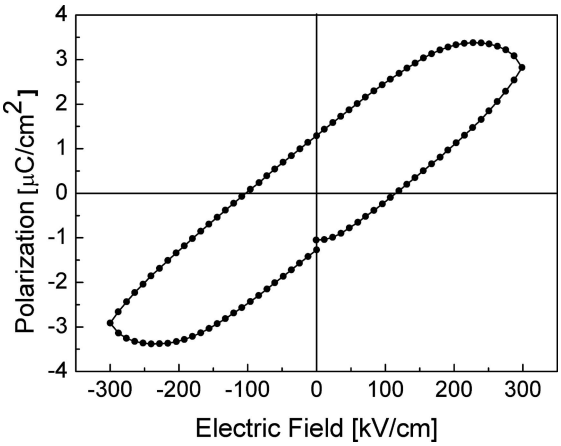


**Fig. 5** Polarization hysteresis curve of a UVP film, obtained at room temperature and triangular voltage pulses of 0.2 ms. Film thickness was 250 nm

NP (see Fig. 6(a)) prevented any meaningful measurement of the C-V-curve. There is a clear evidence for ferroelectric switching as may be inferred from the shape of the curve for UVP. The dielectric constant is highest at the coercive field which points to a strong contribution to the dielectric constant from the dynamics of ferroelectric domains. At higher applied fields the dielectric constant decreases due the domain growth. This behaviour is very much similar to that found for PZT thin films [25, 26]. However, it can be noticed that there is a strong field asymmetry of the curves which are shifted towards negative voltages. This is supposed to be due to the existence of an internal bias field, the origin of which is unclear at this stage.

The ferroelectric hysteresis curve for a 250 nm thick UVP film is shown in Fig. 5. Unfortunately poor polarization properties are obtained under the measuring conditions of the commercial ferroelectric tester, and the curve rather resembles that of a leaky dielectric. We suppose that such a

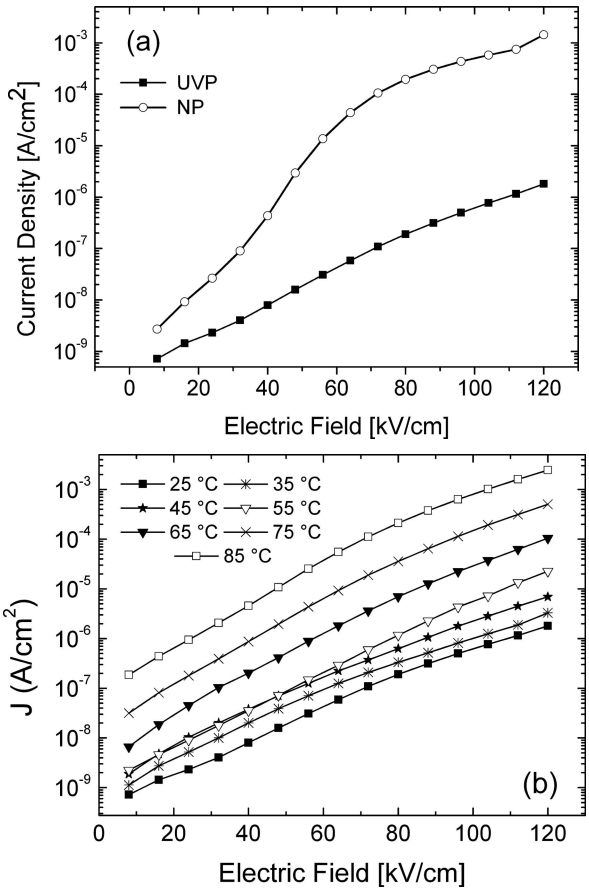


**Fig. 6** (a) Comparison of leakage current densities of UVP and NP specimens at room temperature. (b) Temperature dependence of the leakage current density of UVP. Film thickness was 250 nm

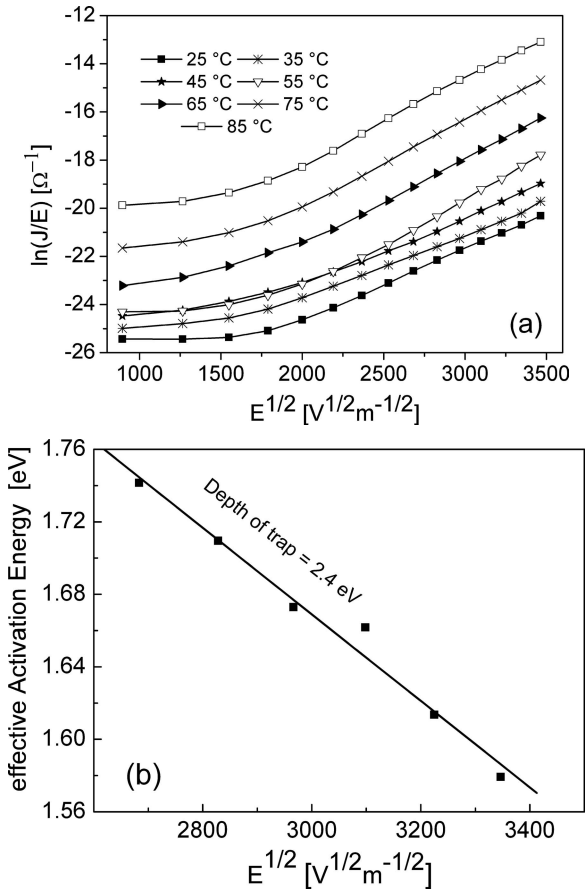


**Fig. 7** (a) Plots of the leakage current density of UVP in Frenkel-Poole coordinates (log $J/E$) vs. $E^{1/2}$ and (b) effective conduction activation energy $E_a$ vs. $E^{1/2}$ showing the linear behaviour and the effective trap depth obtained by extrapolation to $E = 0$

result is the consequence of the measuring method, which uses triangular voltage pulses of 0.2 ms, and could lead to electrical deterioration of the thin film.

### 3.3 Leakage current properties

A comparison of the leakage current densities for UVP and NP is illustrated in Fig. 6(a). It is evident that UV assisted processing improves the leakage current resistance of BFO films by several orders of magnitude. The leakage currents have been measured as function of temperature for UVP, and are illustrated in Fig. 6(b). Conduction in ferroelectric thin films may be analyzed in terms of different mechanisms, including interface limited, e.g. Schottky, and bulk limited, e.g. Frenkel-Poole. In general it is quite difficult to separate these mechanisms as pointed out by Al-Shareef et al. [27], and in our previous work [13]. However, due to the defect structure of BFO, which may include $Fe^{2+}$ and oxygen vacancies [10, 28], it is more likely that a Frenkel-Poole mechanism of conductivity may be operating. The data below were therefore analyzed in terms of the latter mechanism, which can be described by Eq. (1) [24].

$$J \propto E \exp\left[\frac{-q(\phi_B - \sqrt{qE/\pi\varepsilon})}{k_B T}\right], \tag{1}$$

where $E$ is the electrical field, $q$ the elemental charge, $T$ the absolute temperature, $\phi_B$ the trap height, $\varepsilon$ the optical frequency dielectric constant and $k_B$ the Boltzmann constant. According to Eq. (1), $\ln(J/E)$ should be linear with $E^{1/2}$, which is true in a wide range of voltages, as displayed in Fig. 7(a). Effective activation energies of conductivity, $E_a$, at various applied bias fields were found from linear fits of $\ln(J/E)$ vs. $T^{-1}$ (not shown). Figure 7(b) illustrates the nice linear dependency of $E_a$ on $E^{1/2}$ which on extrapolation leads to a trap depth of 2.4 eV. This value is much higher than that obtained in a previous work [13] with a less optimized sol-gel processing, resulting in coarser grained films. An estimation of the ionization energy of $Fe^{2+}$ to $Fe^{3+}$ using enthalpies of formation of $Fe_2O_3$ and FeO yields a value of approximately 3 eV which takes a lower value upon considering entropy contribution. Although qualitative these considerations give a hint as to the conduction mechanisms of BFO, which might involve creation of $Fe^{2+}$ deep traps.

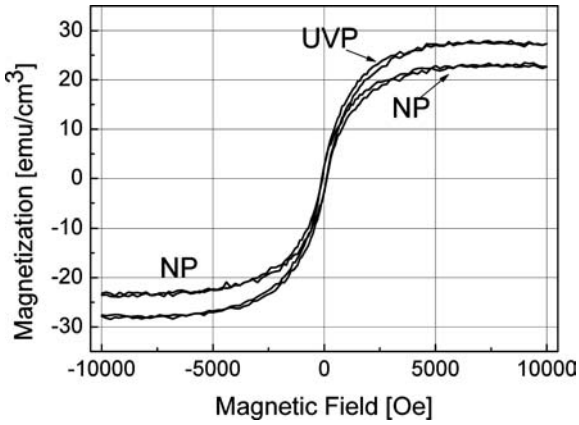


**Fig. 8** Magnetization vs. magnetic field at room temperature for both UVP and NP BFO thin films

### 3.4 Magnetic properties

Finally the magnetic properties were characterized, and are illustrated in Fig. 8 for both UVP and NP specimens. Well saturated magnetization curves with a remnant magnetization of 2Mr of 5.4 emu/cm$^3$ and fairly low coercive fields 2Hc in the range of 200 Oe were obtained. There is evidence as to the beneficial effects of UV assisted pyrolysis on the saturation magnetization, 2Ms, of BFO with values of 55.4 emu/cm$^3$, in comparison to 45.8 emu/cm$^3$ for NP. These values of 2Mr and 2Hc agree to a large extent with those reported for BFO thin films processed via PLD on $SrTiO_3/SrRuO_3$ [4], and are superior to those obtained on platinized silicon substrates [14]. The present results constitute a premiere for the magnetization properties of sol-gel BFO films, and it is quite interesting to note that while the ferroelectric polarization of sol-gel films remains poor, the magnetization properties lie in the range of those of heteroepitaxial films. The polarization switching properties are very sensitive to conductivity which still needs to be substantially decreased for sol-gel films in order to obtain saturation polarization, whereas the magnetic properties, which rely on different switching mechanisms, seem to match those of PLD films.

## 4 Concluding remarks

In conclusion the effects of processing conditions on microstructure, electric and magnetic properties are reported for chemical solution deposited $BiFeO_3$ thin films on (111)Pt/Ti/$SiO_2$/Si substrate heterostructure. The results of hot-plate pyrolysis in air and UV-assisted pyrolysis in oxygen are compared. It is shown that UV-assisted pyrolysis leads to a well crystallized, fine and homogenous grain structure with pronounced (100) texture. The leakage current could be reduced by several orders of magnitude in comparison to hot plate pyrolysed specimens. C-V-curves could be obtained for UV pyrolysed specimens, and their shape suggests polarization switching. The leakage current mechanisms were investigated as a function of temperature, and could be interpreted in terms of Frenkel-Poole mechanism with a trap depth of 2.4 eV. Finally, well shaped and saturated magnetization hysteresis loops were obtained for both processing conditions, and it was shown that UV assisted pyrolysis leads to slightly higher saturation magnetization.

**Acknowledgments** The authors thank the DFG, Grant # ES 119/6-1, for financial support of this work.

## References

1. Roginskaya YE, Venevtsev YN, Fedulov SA, Zhdanov GS (1964) Sov Phys Crystallogr 8:490
2. Kiselev SV, Kshnyakina AN, Ozerov RP, Zhdanov GS (1964) Sov Phys Solid State 5:2425
3. Kubel F, Schmid H (1990) Acta Cryst B46:698
4. Wang J, Neaton JB, Zheng H, Nagarajan V, Ogale SB, Liu B, Viehland D, Vaithyanathan V, Schlom DG, Waghmare UV, Spaldin NA, Rabe KM, Wuttig M, Ramesh R (2003) Science 299: 1719
5. Yang SJ, Zavaliche F, Mohaddes-Ardabili L, Vaithyanathan V, Schlom G, Lee YJ, Chu YH, Cruz MP, Zhan Q, Zhao T, Ramesh R (2005) Appl Phys Lett 87:102903
6. Lee Y-H, Wu J-M, Chueh Y-L, Chou L-J (2005) Appl Phys Lett 87:172901
7. Tyholdt F, Jørgensen S, Fjellvåg H, Gunnæs AE (2005) J Mater Res 20:2127
8. Uchida H, Ueno R, Nakaki H, Funakubo H, Koda S (2005) Jpn J Appl Phys 44:L561
9. Singh SK, Ishiwara H (2005) Jpn J Appl Phys 44:L734
10. Singh SK, Ueno R, Funakubo H, Uchida H, Koda S, Ishiwara H (2005) Jpn J Appl Phys 44:8525
11. Iakovlev S, Solterbeck C-H, Kuhnke M, Es-Souni M (2005) J Appl Phys 97:094901
12. Qi X, Dho J, Tomov R, Blamire MG, MacManus-Driscoll J-L (2005) Appl Phys Lett 86:062903
13. Yakovlev S, Zekonyte J, Solterbeck C-H, Es-Souni M (2005) Thin Solid Films 493:24
14. Yun KY, Noda M, Okuyama M, Saeki H, Tabata H, Saito K (2004) J Appl Phys 96:3399
15. Chang SJ, Lee JS, Wei MC, Chen JF, Liu CH, Liaw UH (2002) J Vac Sci Technol A20:107
16. Calzada ML, Bretos I, Jimenez R, Guillon H, Pardo L (2004) Adv Mater 16:1620
17. Habouti S, Solterbeck C-H, Es-Souni M (2006) Appl Phys Lett in press
18. Lotgering FK (1959) J Inorganic Nuclear Chem 9:113
19. Kumar SR, Habouti S, Zaporojtchenko V, Es-Souni M (2006) J Sol-Gel Sci Tech, in press
20. Chen S-Y, Chen I-Wei (1998) J Am Ceram Soc 81:97
21. Fé L, Norga GJ, Wouters DJ, Maes HE, Maes G (2001) J Mater Res 16:2499
22. Yun KY, Noda M, Okuyama M, Saeki H, Tabata H (2004) In: Hoffmann-Eifert Susanne, Funakubo H, Joshi V, Kingon AI, Koutsaroff IvoP (eds) Ferroelectric thin films XII. Materials Research Society, Pittsburgh, C11.52.1

23. Makoed II, Danil kevich MI (1998) Inorg Mater 34:737
24. Kwan CK (2004) Dielectric phenomena in solids. Elsevier Academic Press, London
25. Hiboux S, Muralt P, Maeder T (1999) J Mater Res 14: 4307
26. Es-Souni M, Piorra A, Solterbeck C-H, Iakovlev S, Abed M (2002) J Electroceram 9:125
27. Al-Shareef HN, Kingon D (1997) J Am Ceram Soc 80:3127
28. Wang YP, Zhou L, Zhang MF, Chen XY, Liu JM, Liu ZG (2004) Appl Phys Lett 84:1731